analytical chemistry

pubs.acs.org/ac Article

Highly Selective Electrochemiluminescence Chemosensor for Sulfide Enabled by Hierarchical Reactivity

Kyoung-Rok Kim, Jinrok Oh, and Jong-In Hong*

Cite This: *Anal. Chem.* 2022, 94, 5091−5098 Read Online

ACCESS | Metrics & More | Article Recommendations | Supporting Information

ABSTRACT: Hydrogen sulfide (H_2S) is a well-known toxic gas with the odor of rotten eggs. Several reaction-based electrochemiluminescence (ECL) chemosensors for H_2S have been developed; however, no homogeneous ECL probe with high selectivity toward H_2S in aqueous media has been reported. Herein, we report an iridium(III) complex-based ECL chemodosimetric probe employing two 7-nitrobenz-2-oxa-1,3-diazol-4-yl (NBD) groups known as a photo-induced electron transfer quencher and a reaction site for the selective detection of H_2S; the detection mechanism involves H_2S being clearly distinguished from biothiols based on the different cleavage rates of the two NBD groups and extremely weak ECL interferences caused by reaction by-products. The probe was rationally designed to improve selectivity toward H_2S within the ECL analysis platform by enabling the removal of nonspecific background signals observed *via* fluorescence analysis. This analytical system exhibited remarkable selectivity toward H_2S, a rapid reaction rate, and high sensitivity (LOD = 57 nM) compared to conventional fluorescence methods. Furthermore, the probe could successfully quantify H_2S in tap water samples and commercial ammonium sulfide solutions, which demonstrates the effectiveness of this probe in field monitoring.

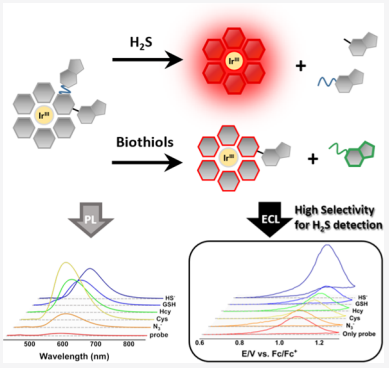

Hydrogen sulfide (H_2S) is a signaling molecule that plays an important role in various biological processes including apoptosis, inflammation, angiogenesis, vasodilation, and neuromodulation.[1] As an anaerobic decomposition product of organic materials, it is also produced primarily in oil and gas industries, agriculture, sewage, and animal waste disposal.[2] Following carbon monoxide, it is the second most toxic gas, causing mortality in humans.[2,3] Chronic exposure to low concentrations of H_2S leads to disorders of the central nervous, respiratory, cardiovascular, and ocular systems.[4] However, inhalation of more than 500 ppm H_2S can cause permanent brain damage, coma, or even death.[5] According to the World Health Organization, the maximum permissible concentration of H_2S in drinking water is 1.47 μM.[6] Therefore, the development of a real-time and accurate detection method for H_2S is necessary.

Various H_2S detection methods, such as gas chromatography,[7,8] high-pressure liquid chromatography,[9−11] and electrochemical analysis,[12−14] have been developed to date. Fluorometric[15−18] and colorimetric[19−21] assays using a single-molecule receptor or probe are of particular interest because of their high sensitivity, selectivity, and rapid detection. However, these conventional methods are not suitable for the real-time detection of H_2S because they require bulky equipment, complicated procedures, and specific conditions. Recently, the electrochemiluminescence (ECL) assay has received much attention because of its high sensitivity and low background signal. Furthermore, it does not require complicated procedures, complex conditions, or large equipment for analysis.[22−25] Therefore, the ECL sensing system is considered a powerful technique for on-site real-sample monitoring, and several research groups have recently sought to develop systems that combine ECL analysis and chemosensors.[26−46] In this regard, an ECL-based detection system in combination with a molecular probe represents a viable option for the development of an efficient on-site H_2S sensing system.

Thus far, several ECL chemosensors for the detection of H_2S based on metal displacement, reduction, and nucleophilic substitution reactions have been developed (Table S1). A ruthenium(II) complex appended with a dipicolylamine−Cu^{2+} complex was reported by Ye et al.[32] Hong *et al.* have developed three ECL probes for H_2S based on iridium(III) complexes.[36,41,42] However, despite their satisfactory performance in the detection of H_2S, their applicability is limited because of the requirement for additional electrode modification procedures, a turn-off response, the requirement for a nonaqueous sensing medium, and low selectivity at low concentrations. Therefore, new ECL probes are required to

Received: December 8, 2021
Accepted: March 10, 2022
Published: March 18, 2022

https://doi.org/10.1021/acs.analchem.1c05317
Anal. Chem. 2022, 94, 5091−5098

Scheme 1. Synthetic Route to (a) Ligands and (b) Probes

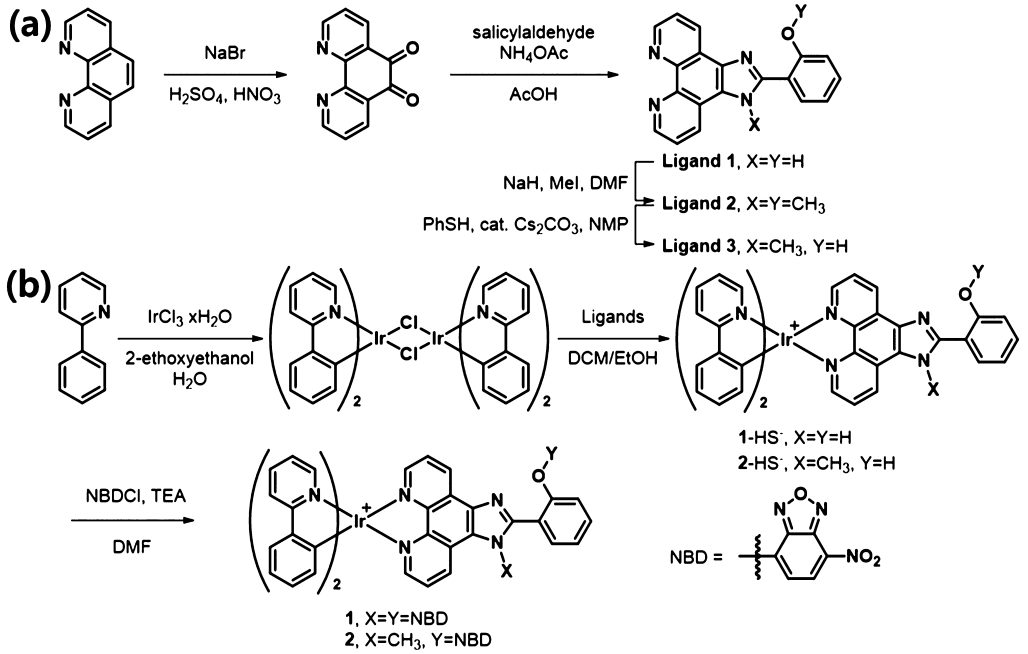

address these drawbacks and satisfy the demand for the rapid, sensitive, and selective detection of H_2S.

Herein, we report a new ECL probe **1** for the selective detection of H_2S over various analytes, including biothiols, based on a cyclometalated iridium(III) complex employing two 7-nitrobenz-2-oxa-1,3-diazol-4-yl (NBD) groups with hierarchical reactivity. Probe **1** displayed a rapid reaction rate, high sensitivity, and remarkable selectivity toward H_2S, suggesting the possibility for field monitoring. To the best of our knowledge, our ECL H_2S analysis system represents the first strategy for removing nonspecific background signals observed in fluorescence analysis.

EXPERIMENTAL SECTION

Materials and Instruments. All the chemicals were purchased from Sigma-Aldrich (Sigma-Aldrich Corp., MO, USA), Tokyo Chemical Industry (TCI, Tokyo, Japan), or Alfa (Alfa Aesar, MA, USA) and were used without further purification. Organic solvents were purchased from Samchun Chemical Co., Seoul, Korea. Thin-layer chromatography (TLC) was performed on TLC plates (aluminum sheets coated with Merck silica gel 60 F-254). Silica gel 60 (230−400 mesh) from SILICYCLE was used as the stationary phase in column chromatography. Deuterated solvents for nuclear magnetic resonance (NMR) spectra were purchased from Cambridge Isotopic Laboratories (Cambridge, MA, USA). All the ^1H and ^{13}C NMR spectra were recorded using a 400 MHz DD2MR400 Agilent NMR system or a Varian 500 MHz NMR system. The chemical shifts of the NMR spectra were recorded in parts per million (ppm), calibrated using the residual solvent signals as an internal reference. High-resolution mass spectrometry (HRMS) data were obtained using a Thermo Scientific Orbitrap Exploris 120 mass spectrometer coupled to a Thermo Scientific Vanquish Core HPLC system. Matrix-assisted laser desorption ionization time-of-flight (MALDI-TOF) mass spectra were obtained using a Microflex from Bruker Daltonics. Ultraviolet−visible (UV−vis) absorption spectra were recorded using a JASCO V-730 spectrometer. The photoluminescence (PL) spectra were measured using a JASCO FP-8300 spectrometer and a SpectraMax M2 spectrophotometer. Both the excitation and emission band widths were 5 nm, except for those recorded using the SpectraMax M2 spectrophotometer (sensitivity: high, 30). Stock solutions of probes (2 mM) were prepared in dimethyl sulfoxide (DMSO) and diluted with deionized water and acetonitrile (CH_3CN). Stock solutions of various anions (10 mM) were prepared in a 10 mM 2-[4-(2-hydroxyethyl)-1-piperazinyl]-ethanesulfonic acid (HEPES) buffer solution (pH 7.40). Sodium hydrosulfide (NaHS) was used as the hydrogen sulfide source in all the experiments. Considering the pK_{a1} of H_2S (7.04), an aqueous H_2S solution largely exists in two forms, with a 7:3 ratio of HS^- and H_2S at pH 7.4.[47]

Electrochemical and Electrochemiluminescent Measurements. To investigate the electrochemical properties, cyclic voltammetry (CV) with a scan rate of 0.1 V/s was performed on individual samples using a CH Instruments 650 B electrochemical analyzer (CH Instruments, Inc., TX, USA). All the redox potential values were referenced with respect to the ferrocene/ferrocenium (Fc/Fc^+) redox couple. The ECL signal was measured along with a CV scan (scan range: 0−1.6 V *vs.* Ag/AgCl, scan rate: 0.1 V/s) using a low-voltage photomultiplier tube module (H-6780, Hamamatsu Photonics K.K., Tokyo, Japan) on which a 250 μL in-house-developed ECL flow cell was directly mounted. All the solutions for the ECL experiments contained 100 mM 2-(dibutylamino)ethanol (DBAE) (Sigma-Aldrich) and 0.1 M tetrabutylammonium perchlorate (TBAP) (TCI) as the co-reactant for ECL and the supporting electrolyte, respectively, in a 1:1 (v/v) mixture of CH3CN (ACROS) and an HEPES-buffered solution (0.1 M, pH 7.4). The glassy carbon (GC) working electrode was polished with 0.05 μm alumina (Buehler, IL, USA) on a felt pad. The electrode was then sonicated in a 1:1 (v/v) mixture of distilled H_2O and ethanol (Samchun Chemical) for 5 min and dried using ultrapure N_2 gas for 1 min. The samples for the electrochemical and ECL experiments were freshly prepared

https://doi.org/10.1021/acs.analchem.1c05317
Anal. Chem. 2022, 94, 5091−5098

Scheme 2. (a) Design Strategy of Probe 1 for Discriminating H_2S Over Cys, Hcy, and GSH; (b) Proposed Sensing Mechanism of Probe 1 for the Detection of H_2S Through ECL Analysis

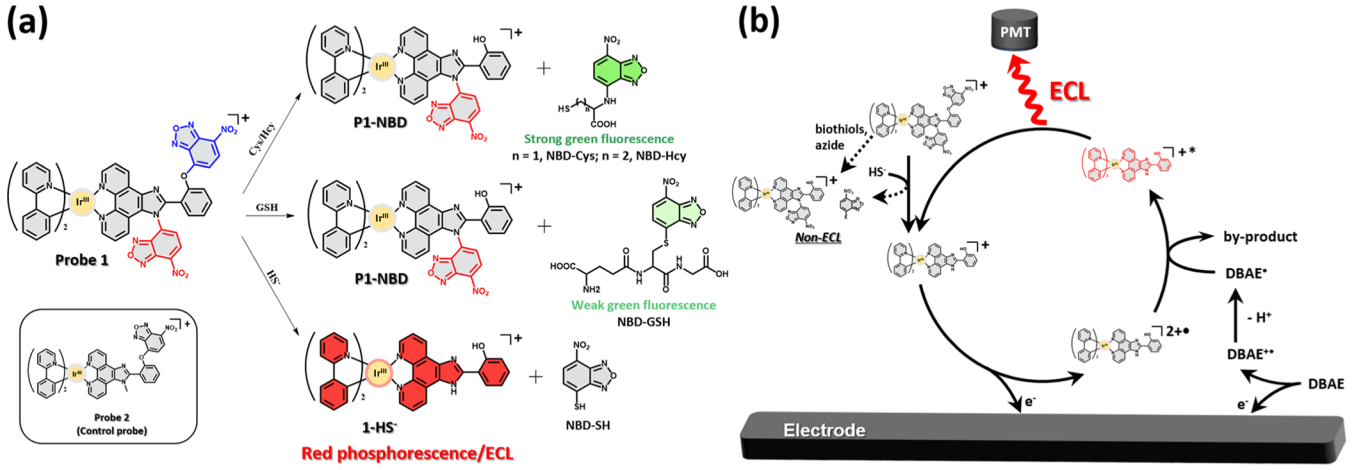

for each experiment. All the ECL data were the average of the values obtained from at least three experiments.

Synthesis of Probes 1 and 2. Probes **1** and **2** were synthesized as shown in Scheme 1. In brief, commercially available 1,10-phenthroline was oxidized to 1,10-phenanthroline-5,6-dione, which was converted into ligand **1** by refluxing in glacial acetic acid in the presence of salicylaldehyde and ammonium acetate. Ligand **1** was successively methylated with iodomethane and then selectively demethylated using a thiophenol−cesium carbonate combination to afford ligands **2** and **3**, respectively (Scheme 2a). The Ir(III) complex dimer with the 2-phenylpyridine (ppy) main ligand was synthesized in refluxing 2-ethoxyethanol at 100 °C. Then, the dimers were chelated using ligands **1** and **3** as ancillary ligands to afford 1-HS^- and 2-HS^-, respectively. Finally, probes **1** and **2** were obtained by introducing an NBD group *via* nucleophilic aromatic substitution (SNAr) in dimethylformamide (DMF) (Scheme 2b). The details of the synthetic procedures and characterization data (^{1}H NMR, ^{13}C NMR, and HRMS) of the new compounds are provided in the Supporting Information.

RESULTS AND DISCUSSION

Design of the Probes. The probes have two components: (i) $[Ir(ppy)_2pip][PF_6]$ (ppy = 2-phenylpyridine, pip = 2-phenyl-1*H*-imidazo[4,5-*f*][1,10]phenanthroline) chosen as the ECL luminophore[48,49] and (ii) an NBD group, a well-known strong electron acceptor, introduced into the ancillary ligand as a photo-induced electron transfer (PeT) quencher and a reaction site for HS^-.[50]

According to our design strategy, the phosphorescence and ECL of probe **1** are quenched by using two NBD groups on the ancillary ligand *via* a PeT process. Assuming that the C−O bond between NBD and phenoxy O is more polarized and sterically less hindered than the C−N bond between NBD and imidazole N, two NBD moieties of probe **1** are removed sequentially *via* the S_NAr mechanism, whereby the latter is cleaved only by the more nucleophilic H_2S rather than by biothiols. A complete removal of the NBD groups from **1** by H_2S restores the molecular structure of 1-HS^- and its phosphorescence and ECL. Moreover, the high ECL selectivity of probe **1** toward H_2S is expected because of the ECL-inactive nature of the other reaction products, such as P1-NBD, NBD-biothiols [biothiols = cysteine (Cys), homocysteine (Hcy), and glutathione (GSH)], and NBD-SH (Scheme 2a). To prove our hypothesis, we designed probe **2**, which lacks the NBD group at imidazole N.

Based on our design strategy, we propose that probe **1** selectively detects HS^- in combination with ECL analysis (Scheme 2b). Probe **1** is expected to react rapidly with HS^- *via* S_NAr to generate 1-HS^-. Then, 1-HS^- is directly oxidized on the GC electrodes to form $(1\text{-}HS^-)^{+\bullet}$, which enters the excited state $(1\text{-}HS^-)^*$ by accepting an electron from the 2-(dibutylamino)ethanol radical ($DBAE^\bullet$), thereby emitting red ECL.

Photophysical Properties and Sensing Abilities of Probes. We first measured the UV−vis and PL spectra of the probes in the absence and presence of HS^- (Figure 1). The strong absorption bands below 330 nm were assigned to the spin-allowed ligand-centered (^{1}LC) transitions of the ppy and pip ligands. The moderate and broad absorption bands in the range of 350−520 nm were assigned to mixing of the metal-to-ligand charge-transfer (^{1}MLCT and ^{3}MLCT) transitions and ligand-to-ligand charge-transfer (^{3}LLCT and ^{1}LLCT) and ligand-centered (^{3}LC) transitions.[51] After the addition of HS^-, a strong absorption band centered at 545 nm appeared, accompanied by a color change from light yellow to hot pink, which has been observed in many NBD-based H_2S probes.[52] Probes **1** and **2** were essentially nonluminescent due to the effective quenching ability of the NBD moiety. As expected, the PL intensity of probes **1** and **2** after the addition of 50 μM (5 equiv) HS^- showed a 44- and 15-fold increase at 600 nm, respectively. Moreover, the corresponding PL spectrum of **1** + HS^- was almost identical to that of 1-HS^-; this indicates that HS^- successfully displaced the NBD moieties to produce 1-HS^- and nonfluorescent NBD-SH (Figure S1). Subsequently, absorption titration experiments for probes **1** and **2** were conducted using HS^-. The absorbance at 545 nm increased linearly with the concentration of HS^- up to 6 and 4 equiv for **1** and **2**, respectively, and the corresponding limit of detection (LOD, signal-to-noise ratio = 3) were calculated to be 0.73 and 1.29 μM, respectively (Figures S2a,b and S3a,b). The PL intensity of **2** at 600 nm also exhibited a linear correlation with the concentration of HS^- up to 4 equiv; thus, the LOD for HS^- as low as 0.12 μM (Figure S4a,b). By contrast, a nonlinear titration curve was observed for **1**, which reached a plateau (53-fold enhancement) after the addition of 6 equiv of HS^-

https://doi.org/10.1021/acs.analchem.1c05317
Anal. Chem. 2022, 94, 5091−5098

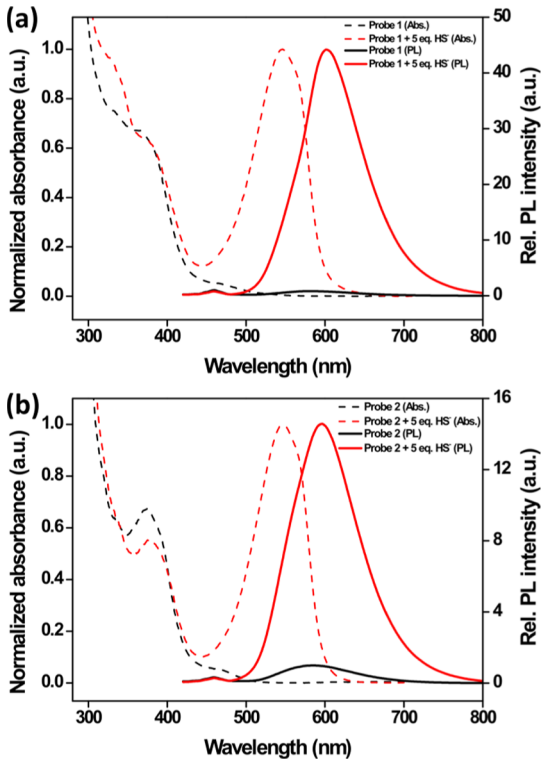

Figure 1. UV−vis absorption (dashed line) and PL spectra (solid lines) of (a) probe **1** (10 μM) and (b) probe **2** (10 μM) before (black) and after (red) the addition of 5 equiv HS^- in CH_3CN/H_2O (1:1 v/v, pH 7.4, 10 mM HEPES).

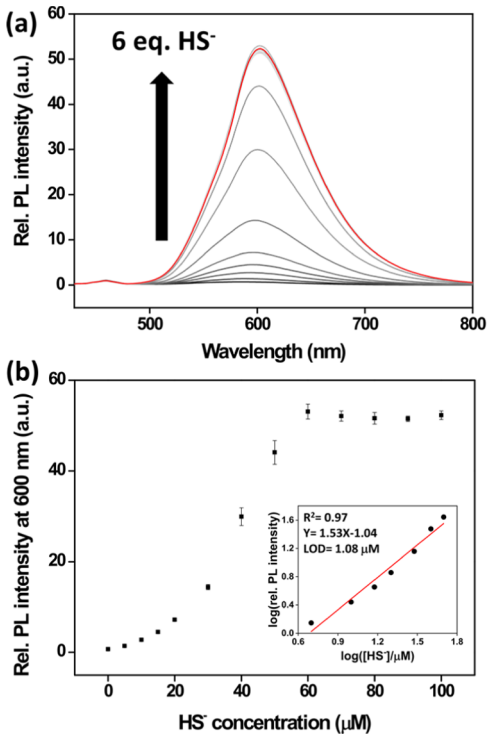

Figure 2. (a) PL emission spectra (λ_{ex} = 400 nm) of probe **1** (10 μM) with increasing HS^- concentrations in CH_3CN/H_2O (1:1 v/v, pH 7.4, 10 mM HEPES) (b) PL intensity changes of probe **1** at 600 nm upon the addition of HS^-. Inset: a linear correlation between log(PL intensity at 600 nm) and log($[HS^-]/\mu M$).

(Figure 2). We hypothesized that this behavior is due to the presence of intermediate species (P1-NBD). Indeed, assuming that (1) two NBD moieties were successively disconnected *via* (2) a bimolecular reaction of probe **1** and HS^- and that (3) the overall intensity could be described as a linear combination of the concentrations of three iridium complexes (**1**, P1-NBD, and **1**-HS^-), the titration curve was successfully fitted using parameters n, k_1/k_2, I_A, I_B, and I_C (Figure S5). The ratios of the intensity parameters (I_C/I_A and I_C/I_B) were in accordance with the turn-on ratios of **1** and **2**, and k_1/k_2 suggested that the first cleavage reaction was much faster than the second one. Although the model could not completely describe the actual reaction that occurred, the reaction was confirmed to comprise two separate steps with different rate constants (see the Supporting Information for details). Meanwhile, a linear correlation between log(PL intensity at 600 nm) and log($[HS^-]/\mu M$) was obtained, and the corresponding LOD was calculated to be 1.08 μM.

Thereafter, the selectivity of the probes toward HS^- was evaluated. The absorbance at 545 nm selectively increased with the addition of HS^-, and the change was linearly dependent on the concentration of HS^-. However, other analytes in excess (10 equiv) failed to induce any significant change at 545 nm (Figures S2c,d and S3c,d), indicating the high selectivity of **1** and **2** for HS^- in UV−vis analysis. However, as shown in Figures 3a and S4c, the PL spectra of **1** and **2** were considerably altered upon the addition of N_3^- and biothiols; this was attributed to the formation of strongly fluorescent NBD-biothiols and NBD-N_3.[50] Therefore, the probes were incapable of discriminating HS^- from other analytes in PL analysis (Figures 3b and S4d).

To obtain a deeper understanding of the sensing mechanism, ^{1}H NMR experiments with probe **1** were performed. In Figure S6, the ^{1}H NMR signals of probe **1** + HS^- are compared with those of **1**-HS^- + HS^-; they clearly indicate that HS^- converted **1** into **1**-HS^- and NBD-SH. In addition, MALDI-TOF analyses of probe **1** with various thiols were performed (Figure S7). As expected, the m/z signal at 1139.8, corresponding to probe **1**, disappeared, and that at 813.5, corresponding to **1**-HS^-, appeared in the presence of HS^-. In contrast, the reaction of probe **1** with biothiols barely proceeded, and only a small amount of P1-NBD was formed. These results demonstrate that the two NBD groups of probe **1** were completely cleaved only in the presence of HS^-.

Finally, we verified the practical applicability of the probes in terms of detection speed and pH susceptibility. The PL intensity of the probes (10 μM) with 50 μM HS^- reached saturation within 2 min, whereas those with 100 μM biothiols required 30 min to 1 h to reach a plateau (Figure S8). Moreover, probe **1** successfully responded to HS^- in the physiological pH range of 6−8; furthermore, the lack of PL changes in probe **1** over a wide pH range of 5−10 confirmed its high stability in aqueous media (Figure S9). The weaker HS^- responses under acidic and basic conditions are presumably due to the low reactivity of HS^- and the deprotonation-induced quenching of **1**-HS^-,[53,54] respectively.

Energy Levels of probe 1 and 1-HS^-. To verify the applicability of the ECL analysis, the electrochemical analysis was performed for probe **1**-HS^- (Figure S10). The electrochemical data are summarized in Table S2. As indicated in Figure S11a, the lowest unoccupied molecular orbital (LUMO) energy level of **1**-HS^- (−3.11 eV) was sufficiently lower than the singly occupied molecular orbital (SOMO)

https://doi.org/10.1021/acs.analchem.1c05317
Anal. Chem. 2022, 94, 5091−5098

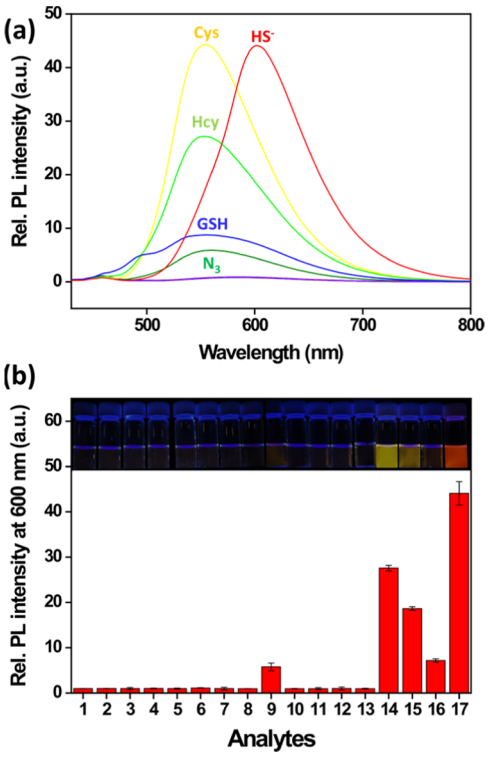

Figure 3. (a) PL emission spectra (λ_{ex} = 400 nm) of probe **1** (10 μM) in the presence of various analytes (100 μM each; HS^-, 50 μM) in CH_3CN/H_2O (1:1 v/v, pH 7.4, 10 mM HEPES). (b) PL emission intensities at 600 nm of probe **1** (10 μM) upon the addition of 100 μM analytes and 50 μM HS^-, [(1) none; (2) F^-; (3) Cl^-; (4) Br^-; (5) $C_2O_4^{2-}$; (6) CN^-; (7) CO_3^{2-}; (8) HCO_3^-; (9) N_3^-; (10) NO_3^-; (11) AcO^-; (12) PO_4^{3-}; (13) SO_4^{2-}; (14) Cys; (15) Hcy; (16) GSH; and (17) HS^-]. Inset: their corresponding photographs taken under 365 nm UV irradiation.

level of the DBAE radical ($DBAE^{\bullet}$); this allowed an electron to be spontaneously transferred from the SOMO of $DBAE^{\bullet}$ to the LUMO of **1**-HS^- to form the excited state for ECL emission. Furthermore, the highest occupied molecular orbital (HOMO) energy level of **1**-HS^- (−5.58 eV) was lower than that of DBAE, which enabled the oxidation of DBAE through the catalytic process for the efficient generation of $DBAE^{+\bullet}$.[55] Thus, probe **1** is expected to possess a high ECL efficiency. Moreover, the relative LUMO level of NBD (−4.08 eV) located between the HOMO (−5.58 eV) and LUMO (−3.11 eV) levels of **1**-HS^- suggested that the phosphorescence of probes **1** and **2** would be quenched by the NBD group *via* the PeT process (Figure S12).

Density functional theory (DFT) calculations were performed for probe **1** and **1**-HS^- using the Gaussian 09 package to determine the structure of the molecular orbitals. The LANL2DZ basis set was used for the iridium atom, while the 6-31G(d,p) basis set was employed for the C, O, N, and H atoms. As shown in Figure S11b, the HOMOs of probe **1** and **1**-HS^- were primarily distributed over the phenyl group of the ppy ligand and the iridium, lying at about −5.6 eV, and the LUMO of probe **1** was distributed on the NBD group lying at −3.83 eV, and the LUMO of **1**-HS^- was mainly localized on the pip ligand lying at −2.43 eV. These results also supported the assumption that the PeT mechanism was responsible for the turn-on response of the probes. To obtain further insight into the optical transitions, we conducted time-dependent DFT calculations based on the optimized molecular geometries at the ground state (S_0) of **1** and **1**-HS^- (Table S3). The energetically lowest singlet vertical excitation ($S_0 \rightarrow S_1$) of probe **1** dominated HOMO → LUMO; this was ascribed to electron transfer (ET) from the main ligand and the iridium center to the NBD group. Moreover, other excitations ($S_0 \rightarrow S_n$, n = 2−8) of probe **1** also exhibited ET characteristics. By contrast, the lowest singlet excitations ($S_0 \rightarrow S_1$) of **1**-HS^- dominated HOMO → LUMO, which was ascribed to the mixing of the ^{1}LLCT and ^{1}MLCT states; this suggests recovery of PL.

ECL Properties of probe 1. We measured ECL intensities with different concentrations of HS^- to verify the sensitivity of probe **1** in ECL analysis. Probe **1** (10 μM) provided stable maximum ECL intensities at 1.11 V (Figure S13) with a gradual increase up to 3.4-fold until 40 μM of HS^- was added (Figure 4a). The LOD was determined to be 57 nM from the

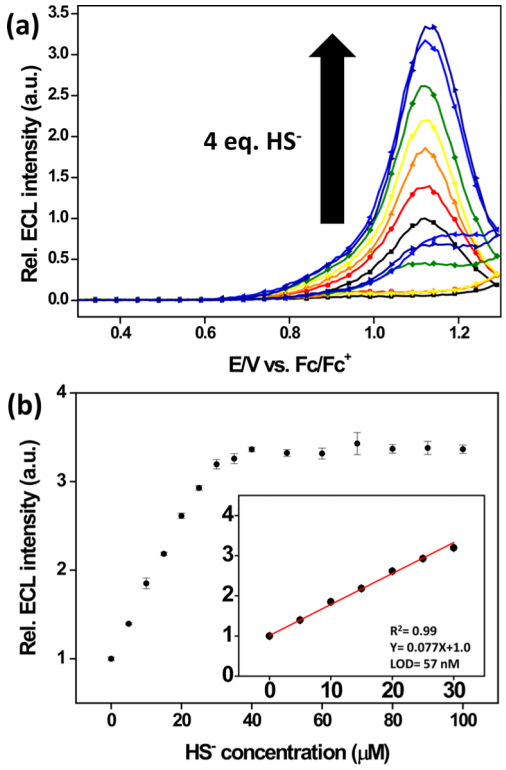

Figure 4. (a) ECL intensities of probe **1** (10 μM) upon the addition of HS^- in CH_3CN/H_2O (1:1 v/v, pH 7.4, 100 mM DBAE, 0.1 M HEPES, and 0.1 M TBAP as the supporting electrolyte) while the potential is swept at a GC disk electrode (diameter 2 mm) in the range of −0.3−1.3 V (scan rate: 0.1 V/s). (b) ECL intensity changes of probe **1** at 1.11 V upon the addition of HS^-. Inset: a linear correlation between the ECL intensity at 1.11 V and concentrations of HS^-.

linear relationship (R^2 = 0.99) between the narrow concentration range of HS^- (0−30 μM) and the ECL intensity (Figure 4b). This LOD value is superior to those (0.73, 1.08 μM) determined from the absorbance and PL analysis (Table S4).

The ECL selectivity of probe **1** for HS^- was also evaluated. As shown in Figure 5a, the addition of 100 μM of various anions and biothiols to probe **1** did not cause any evident change in the ECL intensity. Notably, the strong interferences observed in the PL experiments from highly fluorescent by-

https://doi.org/10.1021/acs.analchem.1c05317
Anal. Chem. 2022, 94, 5091−5098

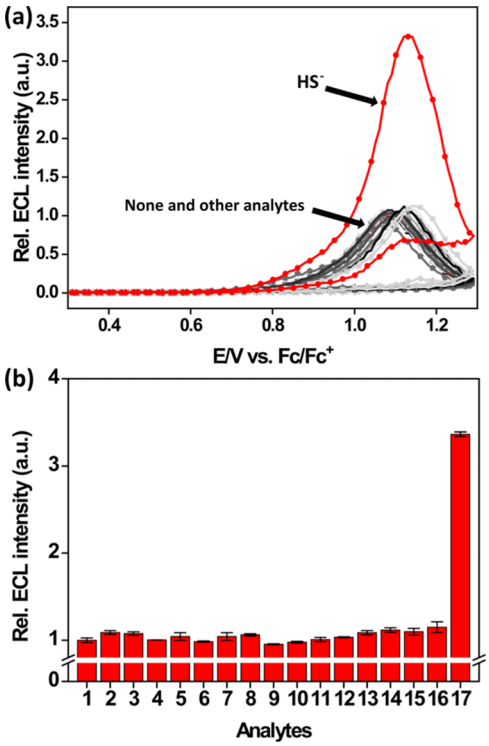

Figure 5. (a) ECL intensities of probe **1** (10 μM) in the presence of various analytes (100 μM each; HS^- 50 μM) in CH_3CN/H_2O (1:1 v/v, pH 7.4, 100 mM DBAE, 0.1 M HEPES, and 0.1 M TBAP as the supporting electrolyte) while the potential is swept at a GC disk electrode (diameter 2 mm) in the range of −0.3−1.3 V (scan rate: 0.1 V/s). (b) ECL intensities at 1.11 V of probe **1** (10 μM) upon the addition of 100 μM various analytes and 50 μM HS^-, [(1) none; (2) F^-; (3) Cl^-; (4) Br^-; (5) $C_2O_4^{2-}$; (6) CN^-; (7) CO_3^{2-}; (8) HCO_3^-; (9) N_3^-; (10) NO_3^-; (11) AcO^-; (12) PO_4^{3-}; (13) SO_4^{2-}; (14) Cys; (15) Hcy; (16) GSH; and (17) HS^-].

products such as NBD-biothiols (biothiols = Cys, Hcy, and GSH) and NBD-N_3 were significantly diminished in the ECL analysis (Figure 5b). This was attributed to the extremely low ECL activities of the organic luminophores (NBD-Cys, NBD-Hcy, NBD-GSH, and NBD-SH) compared with those of the iridium (III) complexes (probe **1** and **1**-HS^-, Figure S14). In contrast, **2** responded not only to HS^- but also to biothiols and N_3^- (Figure S15). Because the addition of HS^- activated the phosphorescence of both probes **1** and **2**, the additional NBD group of probe **1** attached to the imidazole moiety was confirmed to play a crucial role in improving the selectivity toward HS^- in ECL analysis. These results indicate that the ECL assay coupled with probe **1** achieves considerably better performance in terms of selectivity and sensitivity in HS^- detection than the conventional PL system does.

Quantification of HS^- in Water Samples. Quantitative analyses of HS^- in tap water samples using the ECL assay were conducted via a recovery test (Table 1). The concentrations of HS^- in HS^--spiked tap water samples were determined based on the ECL intensities and the calibration curve (Figure 4b). Probe **1** in analytical samples exhibited enhanced ECL intensities upon the addition of HS^-. The recoveries of HS^- were calculated to be 88−98%, and the relative standard deviations were 0.90−2.93%. These results demonstrate that our system has considerable potential for reliable and feasible field monitoring of HS^- in actual samples.

Table 1. Quantification of HS^- in Tap Water Samples[a]

$[HS^-]_{added}$	Rel. ECL intensity (experiment, n = 3)	$[HS^-]_{calc'd}$ (μM)	recovery (%)
5 μM	1.354 ± 0.011	4.420 ± 0.146	88.40 ± 2.93
10 μM	1.770 ± 0.012	9.814 ± 0.151	98.14 ± 1.51
15 μM	2.098 ± 0.012	14.058 ± 0.157	93.72 ± 1.04
20 μM	2.415 ± 0.017	18.175 ± 0.214	90.88 ± 1.07
25 μM	2.847 ± 0.031	23.767 ± 0.401	95.07 ± 1.60
30 μM	3.191 ± 0.021	28.217 ± 0.270	94.06± 0.90

[a]All the ECL intensities were measured along with the CV scan in CH_3CN/H_2O (1:1 v/v, pH 7.4, 100 mM DBAE, 0.1 M HEPES, and 0.1 M TBAP) while the potential was swept at a GC working electrode in the range of −0.3−1.3 V *vs* Fc/Fc^+.

Determination of a Commercial Ammonium Sulfide Aqueous Solution. Ammonium sulfide aqueous solution has been widely utilized in the laboratory and industry for textile manufacturing and photographic film development.[56−58] Increasing the use of ammonium sulfide in the industry generates gaseous and aqueous wastes, resulting in environmental pollution. Furthermore, ammonium sulfide is a poisonous substance with a noisome odor that leads to deleterious effects on humans in both short- and long-term exposure.[59] Therefore, we tested the feasibility of probe **1** for the quantification of sulfide in a commercial aqueous ammonium sulfide solution with a concentration of 0.5−1.0%. The diluted concentration of sulfide was determined by comparing absorbance, PL, and ECL signals with their titration curves (Figures S2b, 2b, and 4b). The actual sulfide concentration by absorbance, PL, and ECL analysis was deduced to be 0.77, 0.73, and 0.55%, respectively, which falls within the range of 0.5−1.0% (Table S5). This quantitative analysis of sulfide in an aqueous solution of ammonium sulfide provides further evidence for the validity and reliability of **1** in real-sample monitoring.

CONCLUSIONS

In this study, a new cyclometalated Ir(III) complex-based ECL chemodosimeter with two reactive sites was developed for the detection of HS^-. To the best of our knowledge, this is the first strategy for removing nonspecific background/interference signals observed in PL analysis using the ECL technique. ECL probe **1** was rationally designed to improve selectivity toward HS^- using the hierarchical reactivity of two reaction sites toward different analytes. The developed system exhibited a rapid reaction rate, sufficient sensitivity (LOD = 57 nM), and remarkable selectivity toward HS^-. Furthermore, the ECL assay coupled with probe **1** could successfully quantify HS^- in tap water samples, which thus represents a new proof-of-concept for the on-site detection of HS^-. We believe that our strategy will be helpful for the development of various ECL sensing systems to detect important small molecules in applications related to biological and environmental sciences.

ASSOCIATED CONTENT

Supporting Information

The Supporting Information is available free of charge at https://pubs.acs.org/doi/10.1021/acs.analchem.1c05317.

Detailed procedures for synthesis, additional UV−vis/PL spectra, MALDI-TOF mass spectra, ECL and CV curves, DFT calculation results, and copies of NMR spectra (PDF)

https://doi.org/10.1021/acs.analchem.1c05317
Anal. Chem. 2022, 94, 5091−5098

AUTHOR INFORMATION

Corresponding Author

Jong-In Hong − *Department of Chemistry, Seoul National University, Seoul 08826, Republic of Korea;* orcid.org/0000-0001-7831-8834; Email: jihong@snu.ac.kr

Authors

Kyoung-Rok Kim − *Department of Chemistry, Seoul National University, Seoul 08826, Republic of Korea*

Jinrok Oh − *Department of Chemistry, Seoul National University, Seoul 08826, Republic of Korea*

Complete contact information is available at: https://pubs.acs.org/10.1021/acs.analchem.1c05317

Author Contributions

All authors have given approval to the final version of the manuscript.

Notes

The authors declare no competing financial interest.

ACKNOWLEDGMENTS

This work was supported by the National Research Foundation grant funded by the Korea Government (MSIT) (no. 2021R1A2C2009088).

REFERENCES

(1) Czyzewski, B. K.; Wang, D.-N. *Nature* **2012**, *483*, 494−497.
(2) Guidotti, T. L. *Handb. Clin. Neurol.* **2015**, *131*, 111−133.
(3) Frame, M. H.; Schandl, C. A. *J. Forensic Sci.* **2015**, *60*, 521−524.
(4) Rumbeiha, W.; Whitley, E.; Anantharam, P.; Kim, D. S.; Kanthasamy, A. *Ann. N.Y. Acad. Sci.* **2016**, *1378*, 5−16.
(5) Balne, P. K.; Sinha, N. R.; Hofmann, A. C.; Martin, L. M.; Mohan, R. R. *Ann. N.Y. Acad. Sci.* **2020**, *1480*, 207−218.
(6) Long, L.; Cao, S.; Jin, B.; Yuan, X.; Han, Y.; Wang, K. *Food Anal. Methods* **2019**, *12*, 852−858.
(7) Hannestad, U.; Margheri, S.; Sörbo, B. *Anal. Biochem.* **1989**, *178*, 394−398.
(8) Vitvitsky, V.; Banerjee, R. *Methods Enzymol.* **2015**, *554*, 111−123.
(9) Wintner, E. A.; Deckwerth, T. L.; Langston, W.; Bengtsson, A.; Leviten, D.; Hill, P.; Insko, M. A.; Dumpit, R.; VandenEkart, E.; Toombs, C. F.; et al. *Br. J. Pharmacol.* **2010**, *160*, 941−957.
(10) Shen, X.; Chakraborty, S.; Dugas, T. R.; Kevil, C. G. *Nitric Oxide* **2014**, *41*, 97−104.
(11) Tan, B.; Jin, S.; Sun, J.; Gu, Z.; Sun, X.; Zhu, Y.; Huo, K.; Cao, Z.; Yang, P.; Xin, X.; et al. *Sci. Rep.* **2017**, *7*, 46278.
(12) Lawrence, N. S.; Davis, J.; Jiang, L.; Jones, T. G. J.; Davies, S. N.; Compton, R. G. *Electroanalysis* **2000**, *12*, 1453−1460.
(13) Dinesh, B.; Shalini Devi, K. S.; Kumar, A. S. *J. Electroanal. Chem.* **2017**, *804*, 116−127.
(14) Hall, J. R.; Schoenfisch, M. H. *Anal. Chem.* **2018**, *90*, 5194−5200.
(15) Lin, V. S.; Chen, W.; Xian, M.; Chang, C. J. *Chem. Soc. Rev.* **2015**, *44*, 4596−4618.
(16) Zhou, X.; Lee, S.; Xu, Z.; Yoon, J. *Chem. Rev.* **2015**, *115*, 7944−8000.
(17) Li, H.; Fang, Y.; Yan, J.; Ren, X.; Zheng, C.; Wu, B.; Wang, S.; Li, Z.; Hua, H.; Wang, P.; et al. *TrAC, Trends Anal. Chem.* **2021**, *134*, 116117.
(18) Geng, Y.; Zhang, G.; Chen, Y.; Peng, Y.; Wang, X.; Wang, Z. *Anal. Chem.* **2022**, *94*, 1813−1822.
(19) Jiménez, D.; Martínez-Máñez, R.; Sancenón, F.; Ros-Lis, J. V.; Benito, A.; Soto, J. *J. Am. Chem. Soc.* **2003**, *125*, 9000−9001.
(20) Hughes, M. N.; Centelles, M. N.; Moore, K. P. *Free Radic. Biol. Med.* **2009**, *47*, 1346−1353.
(21) Chen, H.; Wu, X.; Yang, S.; Tian, H.; Liu, Y.; Sun, B. *J. Anal. Methods Chem.* **2019**, *2019*, 2173671.
(22) Richter, M. M. *Chem. Rev.* **2004**, *104*, 3003−3036.
(23) Miao, W. *Chem. Rev.* **2008**, *108*, 2506−2553.
(24) Hesari, M.; Ding, Z. *J. Electrochem. Soc.* **2015**, *163*, H3116−H3131.
(25) Ma, C.; Cao, Y.; Gou, X.; Zhu, J.-J. *Anal. Chem.* **2020**, *92*, 431−454.
(26) Schmittel, M.; Lin, H.-W. *Angew. Chem., Int. Ed.* **2007**, *46*, 893−896.
(27) Berni, E.; Gosse, I.; Badocco, D.; Pastore, P.; Sojic, N.; Pinet, S. *Chem.—Eur J.* **2009**, *15*, 5145−5152.
(28) Zhang, W.; Zhao, D.; Zhang, R.; Ye, Z.; Wang, G.; Yuan, J.; Yang, M. *Analyst* **2011**, *136*, 1867−1872.
(29) Oh, J.-W.; Kim, T. H.; Yoo, S. W.; Lee, Y. O.; Lee, Y.; Kim, H.; Kim, J.; Kim, J. S. *Sens. Actuators, B* **2013**, *177*, 813−817.
(30) Chen, K.; Schmittel, M. *Chem. Commun.* **2014**, *50*, 5756−5759.
(31) Li, P.; Jin, Z.; Zhao, M.; Xu, Y.; Guo, Y.; Xiao, D. *Dalton Trans.* **2015**, *44*, 2208−2216.
(32) Yue, X.; Zhu, Z.; Zhang, M.; Ye, Z. *Anal. Chem.* **2015**, *87*, 1839−1845.
(33) Li, H.; Sedgwick, A. C.; Li, M.; Blackburn, R. A. R.; Bull, S. D.; Arbault, S.; James, T. D.; Sojic, N. *Chem. Commun.* **2016**, *52*, 12845−12848.
(34) Xu, Y.; Zhang, L.; Liu, Y.; Jin, Z.; Zhao, Q.; Yang, F.; Xiao, D. *Biosens. Bioelectron.* **2016**, *77*, 182−187.
(35) Kim, H. J.; Lee, K.-S.; Jeon, Y.-J.; Shin, I.-S.; Hong, J.-I. *Biosens. Bioelectron.* **2017**, *91*, 497−503.
(36) Kim, S.-Y.; Kim, H. J.; Hong, J.-I. *RSC Adv.* **2017**, *7*, 10865−10868.
(37) Rhee, H.; Kim, T.; Hong, J.-I. *Dalton Trans.* **2018**, *47*, 3803−3810.
(38) Kim, K.-R.; Kim, H. J.; Hong, J.-I. *Anal. Chem.* **2019**, *91*, 1353−1359.
(39) Kim, T.; Hong, J.-I. *ACS Omega* **2019**, *4*, 12616−12625.
(40) Han, D.; Qian, M.; Gao, H.; Wang, B.; Qi, H.; Zhang, C. *Anal. Chim. Acta* **2019**, *1074*, 98−107.
(41) Park, J.; Kim, T.; Kim, H. J.; Hong, J.-I. *Dalton Trans.* **2019**, *48*, 4565−4573.
(42) Kim, H. J.; Kim, T.; Hong, J.-I. *Sens. Actuators, B* **2020**, *307*, 127656.
(43) Kim, T.; Kim, H. J.; Shin, I.-S.; Hong, J.-I. *Anal. Chem.* **2020**, *92*, 6019−6025.
(44) Namkoong, Y.; Oh, J.; Hong, J.-I. *Chem. Commun.* **2020**, *56*, 7577−7580.
(45) Yuan, F.; Hao, K.; Sheng, S.; Fereja, T. H.; Ma, X.; Liu, F.; Zafar, M. N.; Lou, B.; Tian, H.; Xu, G. *Electrochim. Acta* **2020**, *329*, 135117.
(46) Dai, Y.; Zhan, Z.; Chai, L.; Zhang, L.; Guo, Q.; Zhang, K.; Lv, Y. *Anal. Chem.* **2021**, *93*, 4628−4634.
(47) Li, Q.; Lancaster, J. R. *Nitric Oxide* **2013**, *35*, 21−34.
(48) Chen, K.; Schmittel, M. *Analyst* **2013**, *138*, 6742−6745.
(49) Castor, K. J.; Metera, K. L.; Tefashe, U. M.; Serpell, C. J.; Mauzeroll, J.; Sleiman, H. F. *Inorg. Chem.* **2015**, *54*, 6958−6967.
(50) Liu, C.; Liu, J.; Zhang, W.; Wang, Y. L.; Liu, Q.; Song, B.; Yuan, J.; Zhang, R. *Adv. Sci.* **2020**, *7*, 2000458.
(51) Lepeltier, M.; Graff, B.; Lalevée, J.; Wantz, G.; Ibrahim-Ouali, M.; Gigmes, D.; Dumur, F. *Org. Electron.* **2016**, *37*, 24−34.
(52) Ding, S.; Feng, W.; Feng, G. *Sens. Actuators, B* **2017**, *238*, 619−625.
(53) Licini, M.; Gareth Williams, J. A. *Chem. Commun.* **1999**, *19*, 1943−1944.
(54) Zhao, Q.; Zhang, C.; Liu, S.; Liu, Y.; Zhang, K. Y.; Zhou, X.; Jiang, J.; Xu, W.; Yang, T.; Huang, W. *Sci. Rep.* **2015**, *5*, 16420.
(55) Kim, J. I.; Shin, I.-S.; Kim, H.; Lee, J.-K. *J. Am. Chem. Soc.* **2005**, *127*, 1614−1615.
(56) Chiang, V. L.; Sarkanen, K. V. *Wood Sci. Technol.* **1983**, *17*, 217−226.

(57) Maity, S. K.; Pradhan, N. C.; Patwardhan, A. V. *Chem. Eng. J.* **2008**, *141*, 187−193.
(58) Xu, S.; Tang, L.; Bi, C.; Wang, X.; Lv, Y. *Luminescence* **2010**, *25*, 294−299.
(59) Cai, P.; Song, H.; Lv, Y. *Microchem. J.* **2018**, *138*, 116−121.

https://doi.org/10.1021/acs.analchem.1c05317
Anal. Chem. 2022, 94, 5091−5098